

Synthesis, Crystal Structure, and DFT Study of Ethyl 3-(2,3-Dihydrobenzofuran-5-yl)-2-propenoate

L.-X. Ma^{a,b}, Y. Shi^{a,b}, J.-L. Li^{a,b}, Q. Guo^{a,b}, Z.-X. Zhou^{a,b}, and Z.-Y. Huang^{a,b,*}

^a School of Pharmaceutical Sciences, Guizhou University, Guiyang, 550025 China

^b Guizhou Engineering Laboratory for Synthetic Drugs, Guiyang, 550025 China

*e-mail: 785596957@qq.com

Received September 18, 2022; revised September 29, 2022; accepted October 4, 2022

Abstract—The target compound ethyl 3-(2,3-dihydrobenzofuran-5-yl)-2-propenoate was synthesized by a two-step reaction. A single crystal of this compound was grown in a suitable solvent system, the structure of this compound was confirmed by ¹H and ¹³C NMR, MS, FT-IR, and X-ray single crystal diffraction methods. At the same time, conformational studies and crystallographic analysis of the structure were carried out. The Hirshfeld surface analysis method was used to analyze the intermolecular forces. The crystal structure of the target compound was optimized by density functional theory calculations. The crystal structure after X-ray crystal diffraction was compared with the crystal structure optimized by DFT calculation. The results showed that the single crystal structure determined by X-ray crystal diffraction was consistent with the molecular structure after DFT optimization. In addition, by further studying the molecular electrostatic potential and frontier molecular orbital of the target compound, the molecular physicochemical properties of the target compound are understood.

Keywords: 2,3-dihydrobenzofuran, DFT calculations, single crystal X-ray diffraction

DOI: 10.1134/S1070363222120416

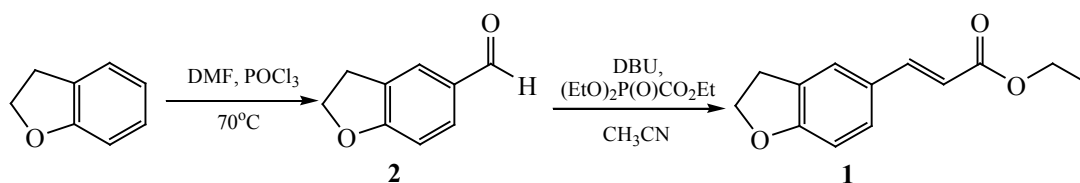
INTRODUCTION

Benzofurans, a class of heterocyclic compounds widely found in nature, have long been the focus of researchers. Heterocyclic compounds with a benzofuran ring as the core have many biological activities, and they are the basic building blocks for drug synthesis and chemical raw materials [1]. The study found that this natural product has novel and diverse structures, broad-spectrum chemotherapeutic properties and diverse pharmacological activities due to the multiple substitution sites on the benzodihydrofuran ring system. Among these pharmacological activities, benzofuran derivatives exhibit nerve growth factor activating activity [2], anti-inflammatory [3, 4], antioxidant properties [5], anti-Alzheimer's disease [6], antibacterial activity [7] and anticancer activity [8]. On the other hand, compounds containing benzofuran structures have been shown to be kinase inhibitors that exert their antiproliferative activities through a variety of cell proliferation inhibitory mechanisms, including induction of apoptosis and inhibition of VEGFR-2 [9]. The structure of 2,3-dihydrobenzofuran contains a saturated five-

membered oxygen heterocycle fused with a benzene ring. Oxygen atoms are adjacent to aromatic systems, and work on the total synthesis of natural products with dihydrobenzofuran ring skeleton has been emerging in recent years.

Ramelteon is a new type of sedative-hypnotic drug with high affinity for melatonin receptors MT1 and MT2, and has been successfully used in the treatment of insomnia patients [10]. Compared with traditional sedative and hypnotic drugs, it has the characteristics of novel mechanism of action, stable efficacy and small side effects. It is currently the drug of choice for the treatment of insomnia with difficulty falling asleep, and it is also the first non-addictive insomnia drug not listed as a special control. In the synthesis of ramelteon, a crucial intermediate, ethyl 3-(2,3-dihydrobenzofuran-5-yl)-2-propenoate, is required. In view of the above points, the design of this paper is accurate, and a new synthesis method of ethyl 3-(2,3-dihydrobenzofuran-5-yl)-2-propenoate with short synthetic route, high selectivity and high yield is developed. The synthetic route is greener and more economical, and provides

Scheme 1.



reference for the synthesis of other key intermediates of ramelteon. Meanwhile, the structure was characterized by FT-IR, ^1H , ^{13}C NMR, and MS and X-ray single crystal diffraction. The crystal structure of the target compound was optimized by DFT calculation, the molecular static point potential and molecular front of the compound were determined. At the same time, the target compound was subjected to conformational analysis, and the crystal structure measured by X-ray was analyzed using the crystal structure data optimized by the DFT method. It was found that the DFT-optimized compound matched the crystal structure determined by X-ray single crystal diffraction.

RESULTS AND DISCUSSION

In this study, we synthesized the target compound through a two-step reaction, as shown in Scheme 1. The structure of compound **1** was confirmed by ^1H , ^{13}C NMR,

MS and FT-IR spectroscopy. The results are shown in Figs. S1–S4 (see Supplementary Information).

Crystallographic analysis. Next, the crystal structure of the title compound **1** was explored for further analysis the structure of this compound. X-Ray diffraction provides sufficient basic data and structural information to analyze the growth of the crystal structure of compound **1**. The compound **1** crystallizes in monoclinic, space group $P21/c$ with the following unit cell parameters: $a = 7.7467(10)$ Å, $b = 20.339(2)$ Å, $c = 7.7370(10)$ Å, $\beta = 109.374(2)^\circ$, $V = 1150.0(2)$ Å³, $Z = 4$, $T = 293.0$ K, $\mu(\text{MoK}\alpha) = 0.71073$ Å, $d_{\text{calc}} = 1.261$ mg/m³.

One of the factors that affects the stability of the crystal structure is the hydrogen bonding present in the compound. The stability of compound **1** is closely related to hydrogen bonding. As shown in Fig. 1, The molecular packing that constitutes the crystal structure is formed by

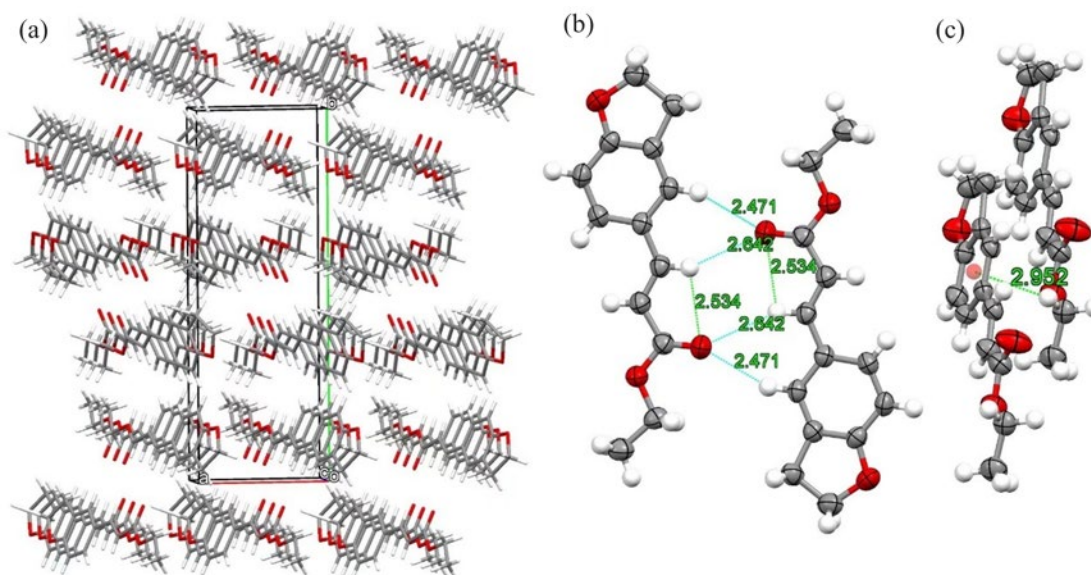


Fig. 1. The crystal packing (a), distance of the hydrogen bond (b), and C–H \cdots π stacking in title compound **1** (c).

Table 1. Hydrogen-bond geometry of compound **1**

D—H...A	<i>d</i> (D—H), Å	<i>d</i> (H...A), Å	<i>d</i> (D...A), Å	(D—H...A) angle, deg
C ³ —H ³ ...O ² ⁱ	0.93	2.47	3.343(2)	156
C ⁹ —H ⁹ ...O ² ⁱⁱ	0.93	2.54	2.860(2)	101

Symmetry codes: i, $-x, y+1/2, -z+3/2$; ii, $-x+1/2, -y, z-1/2$.

hydrogen bonding and van der Waals forces. Compound **1** have two intermolecular hydrogen bond interactions C³—H³...O² (2.471 Å), C⁹—H⁹...O² (2.534 Å). Table 1 lists the hydrogen bond details of the title compound **1**. From the crystal structure in the figure, it can be seen that there are C—H... π stacking interactions in the crystal. There is a C—H... π stacking interaction between C¹²—H¹² and Cg2 with a centroid-centroid distance of 2.952 Å where Cg2 is C¹—C²—C³—C⁴—C⁵—C⁶ ring.

Conformational determination. The conformation of the molecule severely effects its physical and chemical characteristic. Hence, conformational analysis plays a key role in understanding the structure of molecules. It is well known that molecules have different conformations, and the molecular conformation directly affects the physical and chemical properties of molecules. To further understand the crystal structure of the title compound, we performed conformational analysis [11, 12]. The conformation of the starting material of the title compound was searched by the Spartan 08 program [13] and the MMFF [14] molecular mechanics force field. By analysis we obtained ten possible conformers of the title molecule. We selected the conformations and then full geometric optimization was carried out for these structures acquired by DFT/B3LYP/6-311+G(2d, p) basis sets in Gaussian 09 package [15, 16].

Table 2. Gibbs free energy (*G*), relative Gibbs free energy (ΔG)^a, and Boltzmann weighting factor (*P_i*, %)^b of the conformers of compound **1**

Conformer	<i>G</i> , kcal/mol	ΔG , kcal/mol	<i>P_i</i> , %
1a	-729.507073	0	30.32
1b	-729.506651	0.26480749	19.30
1c	-729.505967	0.694021526	9.28
1d	-729.505906	0.732299386	8.69
1e	-729.505821	0.785637387	7.94
1f	-729.505784	0.808855105	7.63
1g	-729.505692	0.866585648	6.91
1h	-729.505373	1.06676003	4.91
1i	-729.504855	1.391808086	2.82
1j	-729.504614	1.543037008	2.18

^a Related to the most stable conformer.

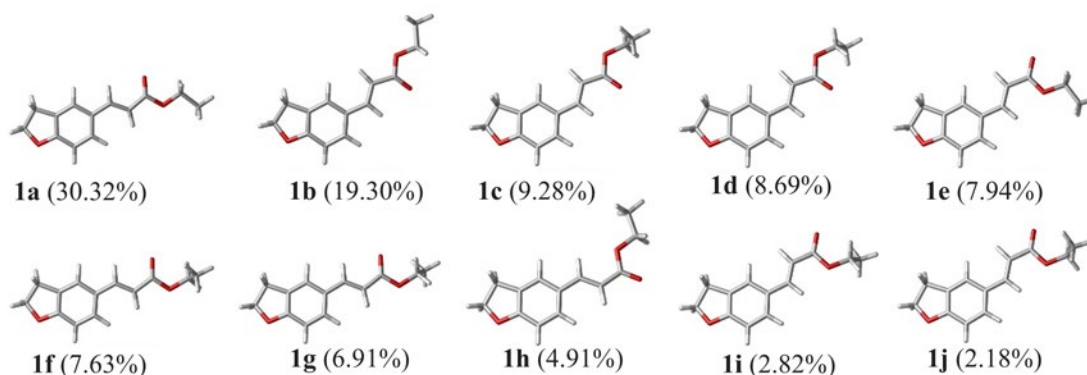
^b Boltzmann weighting factor (*P_i*, %) based on ΔG .

The ratio of each conformer in an equilibrium system is measured at room temperature based on relative free energy. The proportional distribution of conformations in equilibrium mixtures at room temperature can be predicted by relative free energy. The Gibbs free energy (*G*), relative Gibbs free energy (Eq. (1)), and Boltzmann distribution weighting factor, % (Eq. (2)) of each conformation of compound **1** are shown in Table 2.

$$\Delta G = \exp(-G_i/RT), \quad (1)$$

$$P_i = \frac{\exp(-G_i/RT)}{\sum_j \exp(-G_j/RT)} \times 100. \quad (2)$$

For compound **1**, its relatively stable conformation is shown in Fig. 2, respectively. Target compound

**Fig. 2.** Stable conformers of compound **1**.

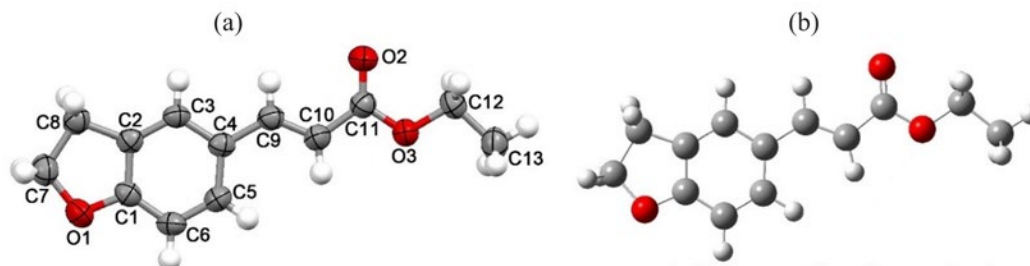


Fig. 3. Crystal (a) and DFT-optimized (b) structures of compound **1**.

1 identified 10 relatively stable conformations: **1a** (32.22%), **1b** (24.97%), **1c** (24.89%), **1d** (10.64%), **1e** (7.28%), **1f** (32.22%), **1g** (24.97%), **1h** (24.89%), **1i** (10.64%) and **1j** (7.28%). The difference between the ten conformations is mainly due to the different orientations of C¹¹ and O³ in the ethyl acrylate group substituted at the C⁴ position of the benzene ring.

The compound crystal optimized by DFT calculation is consistent with the crystal conformation and structure of the **1a** conformation obtained by X-ray diffraction, as shown in Fig. 3.

Molecular electrostatic potential (MEP). The MEP is an important property of molecular systems that allows the determination of the electrophilic reaction region of a compound and the qualitative analysis of the reaction [17]. Electrostatic potential is of great significance for predicting molecular properties, exploring electrostatic interactions between molecules, and predicting reaction sites. In the MEP map, different electrostatic potentials on the surface are represented by different colors, and the

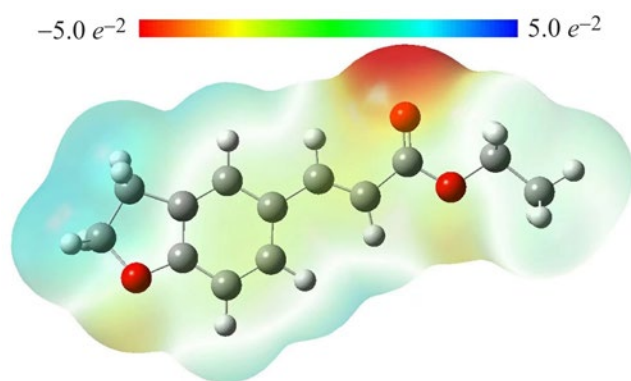


Fig. 4. Molecular electrostatic potential map of conformer **1a**.

potential increases in the order: red < orange < yellow < green < blue [18, 19]. In this paper, the B3LYP/6-311G+(2d, p) method was used to study the MEP of conformer **1a**, and to understand the properties of compound **1**. Intermolecular interaction region information. In the MEP map, the MEP ranges from -5.0 to $5.0 e^{-2}$, and different colors on the molecular electrostatic potential map represent regions with different electrostatic potentials. Among them, red, yellow, green, and blue represent gradual electronegativity lower. The blue area indicates that there is a strong negative electrostatic potential nearby, while the red area indicates that there is a stronger positive electrostatic potential nearby, and the white area has an electrostatic potential close to zero. The red area represents a negatively charged area, a dense area of electrons, which is more prone to attacked by electrophiles, the blue area represents the positively charged area, which is more vulnerable to attack by nucleophiles. As shown in Fig. 4, the H atoms of the C⁷, C⁸ and C¹³ atoms are located in the positively charged region. In addition, the O¹ atom in the dihydrobenzofuran ring and the O² and O³ atoms in the ethyl acrylate group are surrounded by negative charges, indicating a possible nucleophilic attack site at this position point.

Frontier molecular orbitals (FMOs). Frontier molecular orbital studies can effectively demonstrate the prediction of reactivity [20], which determines important chemical properties of compound molecules, such as molecular electron gain and loss and molecular spatial orientation. The chemical reactivity and kinetic stability of molecules can be demonstrated by studying the frontal orbital gap. If the energy gap is small, the molecule has strong reactive properties [21].

First, the highest occupied molecular orbital (HOMO) indicates the degree of relative relaxation of the bonding

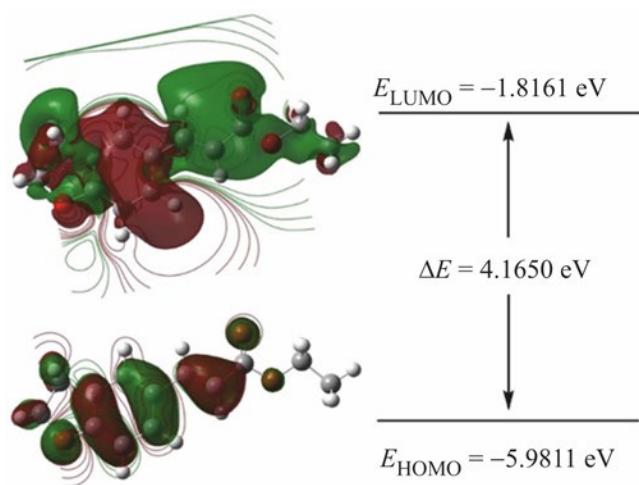


Fig. 5. The HOMO and LUMO of conformer **1a**.

with the electron, which has a stronger activity, and at the same time has the property of electron donor. Second, the lowest unoccupied molecular orbital (LUMO) exhibits a strong affinity for electrons, with electron acceptor properties [22]. The electrons in the frontier molecular orbital are the most sensitive part of the molecule. Molecular orbital theory holds that HOMO and LUMO and their nearby molecular orbitals have the greatest impact on biological activity [23]. To provide important information for identifying active sites and exploring mechanisms of action.

We calculated the HOMO and LUMO energies of conformers **1a** using the B3LYP/6-311+G (2d,p) method to obtain their orbital gaps. As shown in Fig. 5, red and green are used to denote the positive and negative regions of the Frontier Molecular Orbital (FMO). The EHOMO and ELUMO values of conformer **A** are -5.9811 and -1.8161 eV, respectively. The energy interval between HOMO and LUMO is 4.1650 eV, indicating that the compound has good stability. Hardness indicates the compressive strength of a compound [24], which can be expressed as η (3). The hardness of the target compound is 2.0825 eV.

$$\eta = \frac{(-\epsilon_{\text{HOMO}} + \epsilon_{\text{LUMO}})}{2}. \quad (3)$$

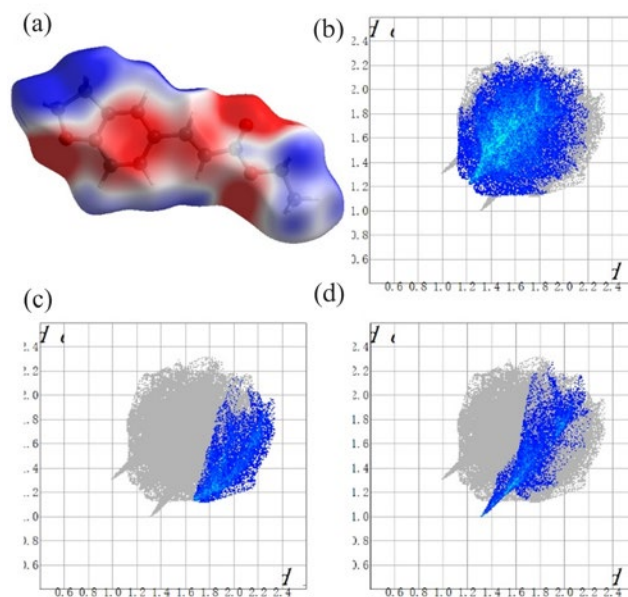


Fig. 6. Hirshfeld surface analyses of **1** mapped with d_{norm} (a), 2D-fingerprint plots for **1** resolved into H \cdots H contacts (b), 2D-fingerprint plots for **1** resolved into C \cdots H contacts (c), and 2D-fingerprint plots for **1** resolved into O \cdots H contacts (d).

Hirshfeld analysis. Two-dimensional fingerprints and Hirshfeld surface analysis were obtained using CrystalExplorer 17.5 [25]. As shown in Fig. 6, The Hirshfeld surface of conformer **1** and the contribution percentages of various modes of action to the Hirshfeld surface. As shown in Fig. 6a, the dark red spots indicate intermolecular hydrogen bonding connections, the white areas indicate connections with longer distances than hydrogen bonds, and the blue areas indicate longer connections relative to the white areas, H \cdots H, C \cdots H and the O \cdots H connections are the three main modes of action. Among them, the H \cdots H effect is distributed in the middle area of the fingerprint, and the contribution to the Hirshfeld surface is the largest, reaching 52.4% , which is the most important mode of action. Followed by the C \cdots H effect, the contribution ratio was 13.3% , and the contribution ratio of the O \cdots H connection was 11.8% .

Vibrational analysis. Infrared spectroscopy is an important instrument for analyzing molecular functional groups. In this article, we performed a vibrational analysis of compound **A** based on the characteristic vibrations of Ar-H, C=O, C=C, C-O-C.

The C-H stretching and bending vibrations on the benzene ring of aromatic compounds consist of multiple strong and weak bands, respectively. There are different

values between 3100 and 2900 cm^{-1} ; the bending vibrations are located at 900–650 cm^{-1} [26], and for the title compound **1**, the tensile and out-of-plane bending vibrations appear at 2980.46 and 816.37 cm^{-1} . This indicates that compound **1** is a benzene ring with two adjacent H.

The stretching vibration of C=O is about 1700 cm^{-1} . For the ester, the carbonyl stretching vibration are absorbed at 1900–1500 cm^{-1} [26], the absorption position of stretching vibration is affected by conjugation effect, resulting in a shift of absorption peaks to lower frequencies. Therefore, compound **1** has stretching vibration at 1732.56 cm^{-1} .

The C=C stretching vibration of benzene ring should be in the range of 1620–1450 cm^{-1} . As long as there is absorption at a place near 1500 or 1600 cm^{-1} , the presence of a benzene ring (or heteroaromatic ring) can be known in principle [26]. Therefore, the tensile vibration of compound **1** may be at 1616.79 cm^{-1} . For olefin, the stretching vibration absorption of C=C is at 1680–1580 cm^{-1} . The stretching vibration of conjugated double bond of compound **1** may occur at 1490.76 cm^{-1} .

The C–O–C stretching vibration peak of the aromatic ether are at 1275–1150 cm^{-1} , and there is also absorption around 940 cm^{-1} , but the intensity is much lower [26]. So, the C–O–C stretching vibration peak of the compound **1** may be at 1155.60.

EXPERIMENTAL

2,3-Dihydrobenzofuran-5-carbaldehyde (**2**).

In a 500 mL three-necked flask dihydrobenzofuran (30 g, 0.250 mol) and *N,N*-dimethylformamide (40.15 g, 0.549 mol) were placed and stirred until dihydrobenzofuran is completely dissolved. Then the solution was cooled on an ice bath to 10°C and phosphorus oxychloride (76.52 g, 0.499 mol) was slowly added dropwise in batches to control the temperature from 30 to 35°C. Phosphorus oxychloride needs to be added within 45 min. The temperature was naturally warmed to room temperature and then slowly raised to 70°C to reflux. After the reaction was completed, the reaction solution was cooled naturally, and then the reaction solution was stirred in crushed ice for 1 h, then extracted with saturated NaCl solution and ethyl acetate, and the organic layer was backwashed three times with saturated aqueous sodium carbonate solution. The organic layer was dried over anhydrous sodium sulfate, filtered with suction, concentrated, and dried to obtain 34.8 g of solid

compound **2** with a yield of 94%. The next reaction was carried out without purification.

Ethyl 3-(2,3-dihydrobenzofuran-5-yl)-2-propenoate (1**).** Anhydrous lithium chloride (2.39 g, 0.331 mol) and triethyl phosphoryl acetate (77.17 g, 0.344 mol) were added to a 250 mL three-necked flask, acetonitrile (100 mL) was added with stirring to dissolve the raw materials, and purged with argon. After cooling to 0°C, 1,8-diazabicycloundec-7-ene (52.4 g, 0.344 mol) was slowly added and stirred for 10 min, the internal temperature was raised to room temperature, and 2,3-dihydrobenzofuran-5-carbaldehyde (34 g, 0.230 mol) was added and reacted at room temperature for 5 h. After the reaction was completed the reaction solution was concentrated, an appropriate amount of water was added, and the reaction solution was extracted with ethyl acetate. The organic layer was dried over anhydrous sodium sulfate, filtered with suction and concentrated to obtain the crude product. Petroleum ether (100 mL) was added to the crude product obtained by rotary evaporation, stirred for 0.5 h, filtered with suction, and dried to obtain 35.52 g of solid compound **1**. Yield 70.93%, mp 53.7–54.6°C. IR spectrum, ν , cm^{-1} : 2980.46 (C_6H_5), 1490.76 (C=C), 1155.6 (C–O–C), 732.56 (C=O). ^1H NMR spectrum, δ , ppm: 1.33 s (3H, CH_3), 3.24 s (2H, CH_2 , dihydrofuran), 4.26 s (2H, CH_2 , dihydrofuran), 4.66 s (2H, CH_2), 6.29 d (1H, CH), 6.79 s (1H, CH), 7.36–7.30 m (1H, C_6H_3), 7.42 s (1H, C_6H_3), 7.65 d (1H, C_6H_3). ^{13}C NMR spectrum, δ_{C} , ppm: 14.36, 29.29, 60.26, 71.81, 77.02, 109.66, 115.08, 124.44, 127.35, 129.47, 144.68, 162.21, 167.45. *M* 219.18.

X-Ray crystal structure determination. The solid of compound **1** was dissolved in acetonitrile, and placed in a clean environment at 15–25°C for 7 days to obtain colorless and transparent crystals. To collect crystallographic data for crystal **1**, X-ray diffraction data were collected on a Bruker APEX-II CCD diffractometer for X-mounted glass fiber crystals with particle sizes of 0.23 mm \times 0.20 mm \times 0.19 mm for compound **1**. Simultaneously, the MoK_α radiation source ($\lambda = 0.71073 \text{ \AA}$) of Bruker APEX II diffractometer was monochromated by graphite at 293 K, and the lattice constant and diffraction intensity of compound **1** crystals were measured. Compound **1** collected 5770 reflections in the range $2.787^\circ \leq \theta \leq 24.994^\circ$ (index range: $-9 \leq h \leq 8$, $-17 \leq k \leq 24$, $-9 \leq l \leq 7$) by φ - ω scan mode and 2021 are independent, $R_{\text{int}} = 0.0265$, of which 146 were observed when $I > 2\sigma(I)$ and were adopted in subsequent

refinements [27]. The structure of compound **1** was solved by directly using the method of SHELXS-2018/3[28], and all data were refined by F^2 full matrix least square method using SHELXL-2018/3. The hydrogen atoms were determined using theoretical calculations, and the final refining result converged to compound **1** with a reliability factor $R = 0.0599$ and a weighted reliability factor $wR = 0.1165$ ($w = 1/[s^2(Fo^2) + (0.0800P)^2 + 0.1100P]$, where $P = (Fo^2 + 2Fc^2)/3$), $(\Delta/\sigma)_{\max} = 0.000$, $S = 1.008$, $\Delta\rho_{\max} = 0.163$ and $\Delta\rho_{\min} = -0.369 e/\text{\AA}^3$.

The crystallographic and processed data are demonstrated in Tables S1 and S2 (see Supplementary Information). Crystallographic data for the title compound have been deposited at the Cambridge Crystallographic Data Centre (CCDC 2151650) and are freely available by visiting the website: www.ccdc.cam.ac.uk/data_Request/cif.

Quantum chemistry/DFT calculation. DFT calculations were performed in the ground state using the Gaussian 09 software package [29] with the B3LYP/6-311+G(2d, p) basis set [30]. Energy, electronic and geometric parameters were obtained from the GaussView 5.0 program [31].

CONCLUSIONS

In this paper, we synthesized ethyl 3-(2,3-dihydrobenzofuran-5-yl)-2-propenoate. The structure of the target compound was confirmed by spectroscopy and mass spectrometry, and the crystal structure was determined by single crystal X-ray diffraction and DFT calculation optimization. The conformational analysis and crystallographic results of the target compound showed that the molecular structure determined by X-ray diffraction matched the molecular structure optimized by DFT calculation. The molecular crystal packing, geometric structure, molecular electrostatic potential, molecular frontier orbital and surface analysis of the target compound crystals were explored and analyzed. Through the comparative analysis of the experimental results and the calculated data, the target ethyl 3-(2,3-dihydrobenzofuran-5-yl)-2-propenoate has good nucleophilic reactivity and good chemical stability. It has great application value in biomedicine.

AUTHOR INFORMATION

Z.-Y. Huang, ORCID: <https://orcid.org/0000-0002-4427-9483>

ACKNOWLEDGMENTS

This work has been awarded the Guizhou Provincial Natural Science Foundation ([2020]1Y393).

CONFLICT OF INTEREST

No conflict of interest was declared by the authors.

SUPPLEMENTARY INFORMATION

The online version contains supplementary material available at <https://doi.org/10.1134/S1070363222120416>.

REFERENCES

- Xu, Z., Zhao, S.J., Lv, Z.S., Feng, L.S., Wang, Y.L., Zhang, F., Bai, L.Y., and Deng, J.L., *Eur. J. Med. Chem.*, 2019, vol. 162, p. 266.
<https://doi.org/10.1016/j.ejmech.2018.11.025>
- Dong, M.Y., Zhang, Y., Jiang, H.Q., Ren, W.J., Xu, L.C., Zhang, Y.Q., and Liu, Y.H., *Eur. J. Med. Chem.*, 2019, vol. 35, p. 5145.
<https://doi.org/10.1080/14786419.2020.1786827>
- Thanika, P., Pawinee, J., Wisanu, M., Roonglawan, R., Sumalee, K., Stephen, G.P., and Thunwadee, L., *Nat. Prod. Res.*, 2020, vol. 34, p. 1394.
<https://doi.org/10.1080/14786419.2018.1512990>
- Kunwar, S., Lee, S.M., Kadayat, T.M., Shrestha, A., Park, P.H., and Lee, E.S., *Bioorg. Med. Chem. Lett.*, 2022, vol. 73, p. 824.
<https://doi.org/10.1016/j.bmcl.2022.128921>
- López-Frias, G., Camacho-Dávila, A.A., Chávez-Flores, D., Zaragoza-Galán, G., and Ramos-Sánchez, V.H., *Molecules*, 2015, vol. 20, p. 8654.
<https://doi.org/10.3390/molecules20058654>
- Ha, H.J., Kang, D.W., Kim, H.M., Kang, J.M., Ann, J., Hyun, H.J., Lee, J.H., Kim, S.H., Kim, H., Choi, K., Hong, H.S., Kim, Y.H., Jone, D.G., and Lee, J., *J. Med. Chem.* 2018, vol. 61, p. 396.
<https://doi.org/10.1021/acs.jmedchem.7b00844>
- Liang, Z., Xu, Z., Tian, Y., Guo, M.B., Su, X., and Guo, C., *Molecules*, 2016, vol. 21, p. 732.
<https://doi.org/10.3390/molecules21060732>
- Gao, Y.T., Ma, C., Feng, X. Z., Liu, Y., and Hai, M.T.X., *Chem. Biodivers.*, 2020, vol. 17, p. 346.
<https://doi.org/10.1002/cbdv.201900622>
- Abdelhafez, O.M., Ali, H.I., Amin, K.M., Abdalla, M.M., and Ahmed, E.Y., *RSC Adv.*, 2015, vol. 5, p. 25312.
<https://doi.org/10.1039/c4ra16228e>

10. Gao, S.Y., Qian, G.Y., Tang, H., Yang, Z., and Zhou, Q.H., *ChemCatChem*, 2019, vol. 11, p. 5762.
<https://doi.org/10.1002/cctc.201901355>
11. Ye, W.J., Chen, D.M., Wu, Q.M., Chen, Y.M., Yang, D.Z., Liao, T.H., and Zhou, Z.X., *J. Struct. Chem.*, 2021, vol. 62, p. 1357.
<https://doi.org/10.1134/s0022476621090043>
12. Zhou, L.P., Qiu, F., Zhang, Z.F., Wang, C.M., Dong, Y.L., and Liu, J.P., *J. Struct. Chem.*, 2020, vol. 61, p. 1111.
<https://doi.org/10.1134/s0022476620070148>
13. Chamberland, S., Ziller, J.W., and Woerpel, K.A., *J. Am. Chem. Soc.*, 2005, vol. 127, p. 755.
<https://doi.org/10.1107/s2053229614024218>
14. Dai, H.Y., Yang, D.Z., Liao, W.P., Wu, F., Zhou, Z.X., and Huang, Z.Y., *Russ. J. Gen. Chem.*, 2022, vol. 92, p. 438.
<https://doi.org/10.1134/s1070363222030112>
15. Wu, Q.M., Zheng, Z.P., Ye, W.J., Guo, Q., Liao, T.H., Yang, D.Z., and Zhou, Z.X., *J. Struct. Chem.*, 2022, vol. 52, p. 1247.
<https://doi.org/10.1016/j.molstruc.2021.131367>
16. Im, G.Y.J., Bronner, S.M., Goetz, A.E., Paton, R.S., Cheong, P.H.Y., Houk, K.N., and Garg, N.K., *J. Am. Chem. Soc.*, 2010, vol. 132, p. 17933.
<https://doi.org/10.1021/ja1086485>
17. Deng, L.Y., Liao, T.H., Sun, H., Hu, W.Y., Zhou, Z.X., Zhao, C.S., and Pan, H.Y., *Mol. Cryst. Liq. Cryst.*, 2022, vol. 737, p. 30.
<https://doi.org/10.1080/15421406.2021.2003952>
18. Wu, Q., Li, J.D., Liu, F.X., Xiao, J.C., Tang, Y.F., and Zi, Q.L., *Russ. J. Coord. Chem.*, 2020, vol. 46, p. 37.
<https://doi.org/10.1134/s1070328420020086>
19. Liu, Y., Zheng, Z., Deng, H., Ren, Q., Zhou, Z., Zhao, C., and Chai, H., *J. Struct. Chem.*, 2021, vol. 62, p. 1285.
<https://doi.org/10.1134/s0022476621080163>
20. Liang, S.Z., Hammond, G.B., and Bo, X., *Eur. J. Med. Chem.*, 2017, vol. 23, p. 17850.
<https://doi.org/10.1080/15421406.2021.2003952>
21. Daoui, S., Çınar, E.B., El Kalai, F., Saddik, R., Dege, N., Karrassi, K., and Benchat, N., *Acta Cryst.*, 2019, vol. 75, p. 1880.
<https://doi.org/10.1107/s2056989019015147>
22. Fukui, K., Yonezawa, T., and Shingu, H.J., *Polym. Sci.*, 1952, vol. 20, p. 722.
<https://doi.org/10.1021/ja1086485>
23. Dyachenko, I.V., Dyachenko, V.D., Yakushev, I.A., Khrustalev, V.N., and Nenaidenko, V.G., *Russ. J. Org. Chem.*, 2020, vol. 56, p. 1669.
<https://doi.org/10.1134/s1070428020090262>
24. Pearson, R.G., *Proc. Natl. Acad. Sci. U.S.A.*, 1986, vol. 83, p. 8440.
<https://doi.org/10.1073/pnas.83.22.8440>
25. Mckinnon, J.J., Fabbiani, F., and Spackman, M.A., *Cryst. Growth Des.*, 2007, vol. 7, p. 755.
<https://doi.org/10.1021/cg060773k>
26. Roberto, G.S.B., *J. Nat. Prod.*, 2005, vol. 66, p. 1577.
<https://doi.org/10.1021/np058254r>
27. Lin, W.Y., Yang, F., Duan, A.N.W., You, W., and Zhao, P.L., *J. Struct. Chem.*, 2018, vol. 37, p. 1557.
<https://doi.org/10.14102/j.cnki.0254-5861>
28. Sheldrick, G.M., *Acta Cryst. (C)*, 2015, vol. 71, p. 467.
<https://doi.org/10.1107/s2053229614024218>
29. Qin, Y., Long, D., Zhu, X., Zhou, Z., Chai, H., and Zhao, J., *J. Struct. Chem.*, 2019, vol. 11, p. 1917.
<https://doi.org/10.1134/s0022476619120072>
30. Vieweg, N., Celik, M.A., Zakel, S., Gupta, V., Frenking, G., and Koch, M., *J. Infrared Millim. Terahertz Waves*, 2014, vol. 35, p. 478.
<https://doi.org/10.1007/s10762-014-0062-3>
31. Wandas, M., Lorenc, J., Kucharska, E., Mączka, M., and Hanuza, J., *J. Raman Spectrosc.*, 2008, vol. 39, p. 832.
<https://doi.org/10.1002/jrs.1922>